

Multilevel beamforming for high data rate communication in 5G networks

Abdoulaye Tall*, Zwi Altman* and Eitan Altman[†]

* Orange Labs 38/40 rue du General Leclerc, 92794 Issy-les-Moulineaux

Email: {abdoulaye.tall,zwi.altman}@orange.com

[†]INRIA Sophia Antipolis, 06902 Sophia Antipolis, France,

Email: eitan.altman@sophia.inria.fr

Abstract

Large antenna arrays can be used to generate highly focused beams that support very high data rates and reduced energy consumption. However, optimal beam focusing requires large amount of feedback from the users in order to choose the best beam, especially in Frequency Division Duplex (FDD) mode. This paper develops a methodology for designing a multilevel codebook of beams in an environment with low number of multipaths. The antenna design supporting the focused beams is formulated as an optimization problem. A multilevel codebook of beams is constructed according to the coverage requirements. An iterative beam scheduling is proposed that searches through the codebook to select the best beam for a given user. The methodology is applied to a mass event and to a rural scenario, both analyzed using an event-based network simulator. Very significant gains are obtained for both scenarios. It is shown that the more dominant the Line of Sight (LoS) component, the higher the gain achieved by the multilevel beamforming.

Keywords

Beamforming, multilevel codebook, Antenna Array, beam focusing, scheduling, 5G network

I. INTRODUCTION

Different solutions and technologies have been developed for focusing transmitted beams on users' receivers, in order to achieve high bit rate communication or tracking capabilities. The technological challenge is twofold: design antenna systems that support narrow beams for large coverage area, and allow to locate users with tight delay constraints for either scheduling or

target tracking. The considerable regain of interest in focusing antennas is related to 5G systems which are in the process of definition in different research frameworks and fora. It is expected that 5G spectrum evolutions will benefit from higher frequency bands [1] making it possible to reduce the size of large antenna arrays.

Different techniques have been developed to focus energy close to the receiver. In an environment rich of multipaths which is typically encountered in dense urban or indoor environment, Time Reversal (TR), also known as the Transmit Matched Filter, is receiving increasing interest, particularly for the internet of things [2]. TR is a pre-filtering technique for Multiple Input Multiple Output (MIMO) wireless systems [3]. The channel state information at several transmit antennas is used to precode transmitted symbols with the time reversed version of their respective channel impulse responses. These "time reversed" waves propagate in the channel, resulting in power focusing in space and time at the receiver. TR can be efficiently used for low complexity receivers such as those expected in future connected objects [4], and even for high mobility scenarios [5]. The drawback of this technique is that it requires Time Division Duplex (TDD) and full Channel State Information (CSI) at the transmitter side.

The problem of focusing the beam on moving targets has been addressed for decades in the context of radar applications, and more specifically, in millimeter wave phase array technology. Recently, the use of millimeter adaptive antenna array, operating at the 70/80 GHz bands, has been proposed for serving a high data rate moving user [6]. The antenna array consists of analog sub-arrays behind a digital beamformer that estimates the Angle of Arrival (AoA) for the moving user.

Multilevel beamforming has been proposed in [7] for millimeter wave backhaul serving urban pico-cells. To ensure the link quality, an efficient search algorithm is performed to maintain the alignment of the transmit and receive beams. The search is performed on a multilevel codebook thus reducing considerably the number of beam couples to be tested. The channel gain matrix is not required, making this technology cheaper and suitable for FDD systems.

Recently, the concepts of Virtual Small Cell (VSC) [8] and Virtual Sectorization (ViS) [9] have been proposed, with the aim of creating a small cell or a sector using an antenna array located at the base station. To manage interference between the macro cell and ViS, a self-optimizing frequency splitting algorithm has been proposed that dynamically shares the frequency bandwidth between the two cells. The main technological challenge for both VSC and ViS is

how to optimally focus the beam at the area where traffic is present. This issue is implicitly solved by the multilevel beamforming proposed in this paper.

The present work adapts the concept of multilevel beamforming to the context of multi-user communication. In terms of implementation complexity, the proposed approach is particularly attractive. It can be implemented in a FDD system where the beam selection only depends on the mobile feedback, namely on the Channel Quality Indicator (CQI). Different scenarios can be envisaged for the multilevel beamforming, such as cellular coverage (in the sense of service provisioning) in a low level or multipath propagation environment or the coverage of mass events and crowded area. Unlike the backhaul problem described above, the multilevel beamforming in this paper is generated at the transmitter only. Cell coverage should be guaranteed with low level inter-cell interference. The projection of beams (particularly high gain narrow beams) may strongly spread out and overshoot neighboring cells. Hence the generation of the set of multilevel beams (or codebook) should take into account geometrical parameters of the cell (e.g. cell size, antenna height) and can be performed off-line.

The contributions of the paper can be summarized as follows:

- An antenna optimization framework for generating beams with reduced interference from side-lobes for large angular domain.
- A beamforming codebook design strategy which avoids overshooting at neighboring cells.
- A beam selection algorithm for efficient search through the multilevel beamforming codebook.
- Performance analysis of the multilevel beamforming for two Long Term Evolution (LTE) use cases taking into account different channel and traffic models.

The rest of the paper is organized as follows. Section II presents the antenna array design and optimization for the multilevel beamforming. Section III describes the multilevel beam construction and their selection algorithm. The performance of the proposed multilevel beamforming for different channel models is analyzed in Section IV for a mass event and a rural scenario using an event-based LTE network simulator. Section V concludes the paper.

II. ANTENNA ARRAY DESIGN

This Section presents the guidelines for the antenna array design supporting multilevel beamforming. The antenna array modeling is first introduced and then the design of the beam diagrams

is formulated as an optimization problem.

A. Antenna model

Consider a $N_x \times N_z$ (sub) antenna array of vertical dipoles, at a distance of $\frac{\lambda}{4}$ from a square metallic conductor, with λ being the wavelength. The full antenna array generates the highest level (narrowest) beams, whereas lower level beams correspond to smaller (rectangular) sub arrays size (see Figure 2). If another type of radiating element is chosen, only its radiation pattern should be modified. To simplify the model, we approximate hereafter the reflector as an infinite perfect electrical conductor (PEC). The N_x and N_z elements in each row and column are equally spaced with distances d_x and d_z , respectively (Figure 1).

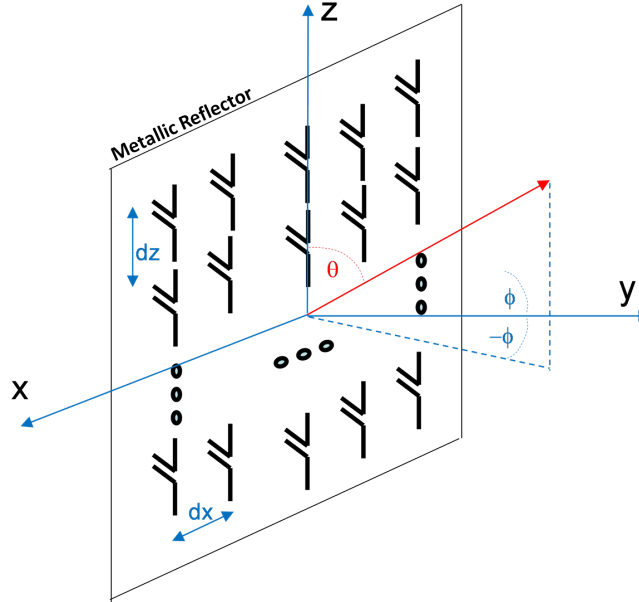


Fig. 1. Antenna array with dipole radiating elements.

The direction of a beam is determined by the angle (θ_e, ϕ_e) in the spherical coordinates θ and ϕ . The antenna gain for a given beam defined by (θ_e, ϕ_e) in a given direction (θ, ϕ) is written as

$$G(\theta, \phi, \theta_e, \phi_e) = G_0 f(\theta, \phi, \theta_e, \phi_e) \quad (1)$$

where f is a normalized gain function and G_0 the maximum gain in the (θ_e, ϕ_e) direction. A separable excitation in the x and z directions is assumed, resulting in the following separable

form of f :

$$f(\theta, \phi, \theta_e, \phi_e) = |AF_x^2(\theta, \phi, \theta_e, \phi_e) \cdot AF_y^2(\theta, \phi) \cdot AF_z^2(\theta, \theta_e)| \cdot G_d(\theta) \quad (2)$$

$AF_x(\theta, \theta_e, \phi, \phi_e)$ and $AF_z(\theta, \theta_e)$ are the array factors in the x and z directions and are given by

$$AF_x(\theta, \theta_e, \phi, \phi_e) = \frac{1}{\sum_{m=1}^{N_x} w_m} \sum_{m=1}^{N_x} w_m \cdot a_m \quad (3)$$

and

$$AF_z(\theta, \theta_e) = \frac{1}{\sum_{n=1}^{N_z} v_n} \sum_{n=1}^{N_z} v_n \cdot b_n. \quad (4)$$

a_m and b_n are complex amplitude contributions of the radiating element located at $(m-1)d_x$ and $(n-1)d_z$, respectively:

$$a_m = \exp\left(-j2\pi \frac{(m-1)d_x}{\lambda} (\sin \theta \sin \phi - \sin \theta_e \sin \phi_e)\right), \quad (5)$$

$$b_n = \exp\left(-j2\pi \frac{(n-1)d_z}{\lambda} (\cos \theta - \cos \theta_e)\right). \quad (6)$$

The weights w_m and v_n for radiating elements in the m -th row and n -th columns define a Gaussian tapering function used to control the sidelobe level of the gain pattern

$$w_m = \exp\left(-\left(\frac{(m-1)L_x - \frac{L_x}{2}}{\sigma_x}\right)^2\right), \quad (7)$$

$$v_n = \exp\left(-\left(\frac{(n-1)L_z - \frac{L_z}{2}}{\sigma_z}\right)^2\right), \quad (8)$$

where L_x and L_z are the array size in the x and z directions respectively, with $L_x = (N_x - 1)d_x$ and $L_z = (N_z - 1)d_z$. The values for σ_s , $s = x, z$, are defined by fixing the ratio between the extreme and center dipole amplitudes respectively to a given value of α_s :

$$\sigma_s^2 = -\left(\frac{L_s}{2}\right) \frac{1}{\log(\alpha_s)}; s = x, z \quad (9)$$

The impact of the PEC can be modeled by replacing it with the images of the radiating elements it creates. The term $AF_y(\theta, \phi)$ takes into account the images and is written as:

$$AF_y(\theta, \phi) = \sin\left(\frac{\pi}{2} \sin \theta \cos \phi\right) \quad (10)$$

The normalized gain pattern of the dipoles, $G_d(\theta)$, is approximated as

$$G_d(\theta) = \sin^3 \theta. \quad (11)$$

The term G_0 is obtained from the power conservation equation:

$$G_0 = \frac{4\pi}{\int_{-\frac{\pi}{2}}^{\frac{\pi}{2}} \int_0^\pi f(\theta, \phi) \sin \theta d\theta d\phi}. \quad (12)$$

A beam is defined by the (rectangular) sub-array size, and the couple (θ_e, ϕ_e) defines its direction. The generation of the beams is discussed in Section III. The antenna modeling for all the beams remains unchanged.

B. Antenna pattern optimization

The (sub) antenna array design constitutes an optimization problem with two objectives: maximizing the antenna gain (or conversely, minimizing the width of the main lobe) and minimizing the side-lobes' level, as a function of the parameters d_s and α_s , $s = x, z$. The problem is written as a constrained optimization problem:

$$\underset{d_x, d_z, \alpha_x, \alpha_z}{\text{maximize}} G_0(N_{x, \max}, N_{z, \max}, d_x, d_z, \theta_e, \phi_e) \quad (13a)$$

$$\text{s.t.} \quad (13b)$$

$$\max_{N_x, N_z} \{SL(N_x, N_z, d_x, d_z, \theta_e, \phi_e)\} \leq Th; \quad (13c)$$

$$N_{s, \min} \leq N_s \leq N_{s, \max}; \quad s = x, z; \quad (13d)$$

$$0 < \alpha_s \leq 1; \quad s = x, z; \quad (13e)$$

$$0 < d_s \leq \frac{\lambda}{2}; \quad s = x, z; \quad (13f)$$

$$\theta_{\min} \leq \theta_e \leq \theta_{\max}; \quad (13g)$$

$$-\phi_{\max} \leq \phi_e \leq \phi_{\max}; \quad (13h)$$

where $N_{s, \min}$ and $N_{s, \max}$ are respectively the minimum and maximum number of antenna elements in the s direction, $\theta_{\min}, \theta_{\max}, \phi_{\min}, \phi_{\max}$ are respectively the minimum and maximum electrical elevation and azimuth angles of the antenna array. The constraint (13c) reads: the maximum side-lobe level for the whole range of sub array size should be below a predefined threshold Th .

It is noted that for small elevation electrical tilt values, the projection of the beams on the plane is likely to spread out. Special care should be taken when setting the $\theta_{\min}, \phi_{\min}, \phi_{\max}$ angles in order to avoid overshooting on neighboring cells. These angles will depend on the geometrical characteristics of the cell (original coverage area of the considered Base Station (BS) before deploying the antenna array), such as the cell shape, size, and antenna height. One can consider optimizing the antenna for a wide range of elevation and azimuth angles, and then, according to the cell geometry, construct a codebook of beams for a desired angular range. Furthermore, a database with a set of codebooks can be pre-optimized for a set of cell geometries and then, according to the specific cell deployment, the most suitable codebook can be selected.

III. MULTILEVEL BEAMFORMING

A. Beams structure

Consider a multilevel codebook as shown in Figure 2, with L levels and J_l beams at the level l , $l = 0, \dots, L$. The j th beam at level l is written as $B_{l,j}(\theta, \theta_{l,j}, \phi, \phi_{l,j})$, $j = 1, \dots, J_l$, and for brevity of notation - as $B_l(j)$. It is noted that the angles $(\theta_{l,j}, \phi_{l,j})$ correspond to (θ_e, ϕ_e) defined in section II.

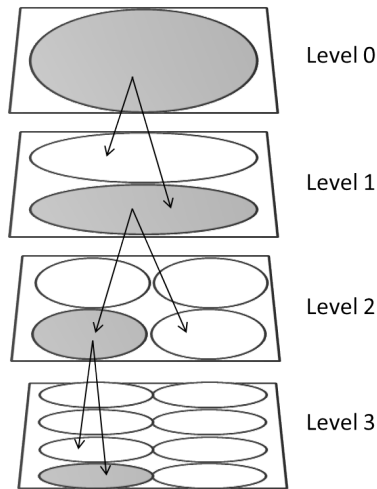


Fig. 2. Example of beam hierarchy

The beam of the first level, namely level 0 in Figure 2, $B_0(1)$, covers the entire cell. Beams at level l are generated by the same sub-array, i.e. with the same number of array elements,

and differ from each other by the angles $(\theta_{l,j}, \phi_{l,j})$. Denote by \hat{C} a *coverage operator* which receives as argument a beam, and outputs its coverage area (often denoted as the best server area), where the beam provides the strongest signal with respect to other cell or beam coverage. By construction we assume that for a given level l , the beams' coverage do not overlap:

$$\hat{C}(B_l(i)) \cap \hat{C}(B_l(j)) = \emptyset, \forall i \neq j. \quad (14)$$

The multilevel structure of the beams in the codebook means that a given beam $B_l(j)$ at level l where $l < L$ has two children beams $B_{l+1}(2j-1)$ and $B_{l+1}(2j)$ with

$$\hat{C}(B_{l+1}(2j-1)) \cup \hat{C}(B_{l+1}(2j)) \subset \hat{C}(B_l(j)) \quad (15)$$

The beams at level L are the narrowest that can be obtained given the $N_{x,max} \times N_{z,max}$ antenna array.

B. Beam selection algorithm

The beam selection algorithm consists in finding the best beam available by navigating through the multilevel codebook. It starts with $B_0(1)$ which covers the entire cell and keeps track of the overall best beam up till now (B^*). Assuming the beam selection algorithm is at level l with $l < L$, the best beam is updated as follows

$$B^* = \underset{B \in \{B^*, B_{l+1}(j), j=(2j_{l+1}-1, 2j_{l+1})\}}{\arg \max} S(B, u) \quad (16)$$

where $S(B, u)$ is the Signal to Interference plus Noise Ratio (SINR) of user u served by the beam B , and j_l denotes index of the beam at level l .

The algorithm stops when the best beam does not change in a given iteration, i.e. the parent beam provides better SINR than the children beams, or the highest level of beams L is reached. The complexity of such an algorithm is of the order of $\log(N)$, N being the total number of beams, hence convergence is obtained in a very small number of iterations.

It is noted that condition (15) can be relaxed so that narrower beams can cover regions not covered by their parent beams. In this case the beam selection algorithm should continue until level L . The multilevel beam structure presented in this section is just one illustration of how a multilevel codebook structure can be designed. Other approaches can be adopted regarding the relation between parent and children beams in terms of coverage. The only requirement is to be able to easily navigate through the codebook in an iterative manner.

The beam selection algorithm runs in parallel with the scheduling algorithm. A user is first scheduled based on its SINR obtained with the level 0 beam. During the scheduling period, the user's best beam is updated based on the received feedback using equation (16). If the scheduling period is long enough, the beam selection algorithm can converge. Otherwise the beam selection resumes at the next scheduling period based on the SINR of the best beam tested so far. It is noted that other scheduling strategies can be considered.

C. Implementation issues

The beam codebook can be precalculated for a given cell and stored in a database of a self-configuration server at the management plane. Upon deployment of the multilevel beamforming feature, the multilevel codebook is downloaded from the server to the BS. As mentioned previously, the codebook selection can be based on geometrical characteristics of the cell.

The antenna array can be dynamically configured using different approaches. The classical approach would be to feed each antenna element by a distinct amplifier which receives the appropriate input signal necessary to excite the selected beam from the codebook. More recently, the *load modulated massive MIMO* approach has been reported [10] in which the base band input signal is used to adapt a load behind each antenna element which controls its complex input impedance. This approach which utilizes a single amplifier aims at further reducing the antenna size and cost, and could be a candidate technology for the multilayer beamforming (further studies are still necessary).

The size of the antenna array depends on the number of antenna elements and the spacing between them. In Section IV-A, we use $N_{x,max} = 12$ and $N_{z,max} = 32$ antenna elements with spacings of $d_x = 0.5\lambda$ and $d_z = 0.7\lambda$. For the LTE technology with a 2.6 GHz carrier, the antenna size is of $0.69 \text{ m} \times 2.58 \text{ m}$. Multilevel beamforming will be particularly attractive in 5G technology where higher frequency bands will be available, allowing moderate size of antenna array with a large number of radiating elements.

IV. NUMERICAL RESULTS

We present in this section numerical results for the multilevel beamforming. Two scenarios are considered: a mass event type of scenario in an urban environment with a crowded open area, e.g. an esplanade, and a rural environment in which the users have a LoS path component

from the BS. The multilevel beamforming is applied to one cell which is interfered by two rings of neighboring BSs.

A LTE event-based simulator coded in Matlab is used. Users (data sessions) arrive according to a Poisson process, download a file of exponential size with mean of 4 Mbits, and leave the network as soon as their download is complete. We focus on the case where there is no mobility. The channel coherence time of several milliseconds is assumed (which is typically the case for low mobility), and so the beam selection algorithm converges within this coherence time. Hence beam selection errors due to fast-fading are not considered.

The main simulation parameters used for the two scenarios are summarized in Table I.

A. Mass event scenario

Consider a cell with a very large hotspot described by a spatial Gaussian traffic distribution which is superimposed on a uniform traffic over the whole cell area as shown in Figure 3. This distribution represents the traffic intensity map in arrivals per second per km^2 . The hotspot can represent a crowd watching a live concert held on an esplanade for example. It is assumed that the users have a significant direct (LoS) path with the BS. It is recalled that in a rich scattering environment, other MIMO techniques are more appropriate. In order to take into account the residual multipaths due to reflections on neighboring buildings, we use the Nakagami-m distribution for the fast fading.

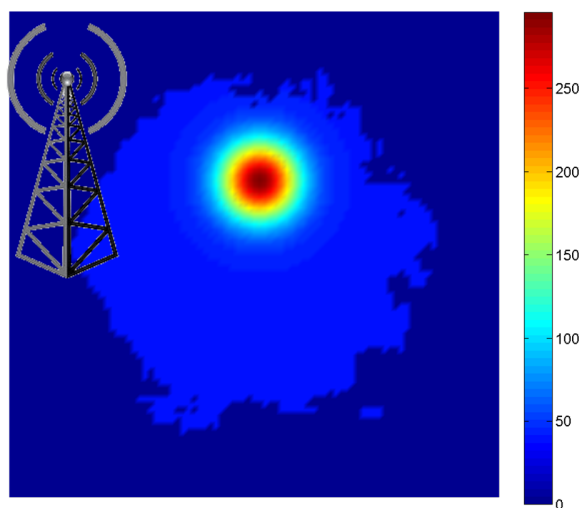


Fig. 3. Traffic intensity map (in users/s/ km^2).

TABLE I. NETWORK AND TRAFFIC CHARACTERISTICS

Network parameters	
Number of sectors with multilevel beamforming	1
Number of interfering macros	2 rings, 20 sectors
Macro Cell layout	hexagonal trisector
Antenna height	30 m
Bandwidth	10MHz
Scheduling Type	Proportional Fair
Channel characteristics	
Thermal noise	-174 dBm/Hz
Path loss (d in km)	$128.1 + 37.6 \log_{10}(d)$ dB
Shadowing	Log-normal (6dB)
Traffic characteristics	
Service type	FTP
Average file size	4 Mbits

1) Illustration of the multilevel beamforming: Figures 4, 5 and 6 represent the coverage maps of the beams in each level, the best beam chosen at each level for a user located at the center of the hotspot area (yellow square in Figure 5) and the corresponding antenna diagrams, respectively, as described below.

The multilevel beam structure presented in Section III is illustrated in Figure 4. Here, the condition (14) is met by definition of the coverage areas. However, condition (15) is relaxed in order to allow narrower beams (level 3 in Figure 4d) to cover blank spaces left by wider beams (level 2 in Figure 4c).

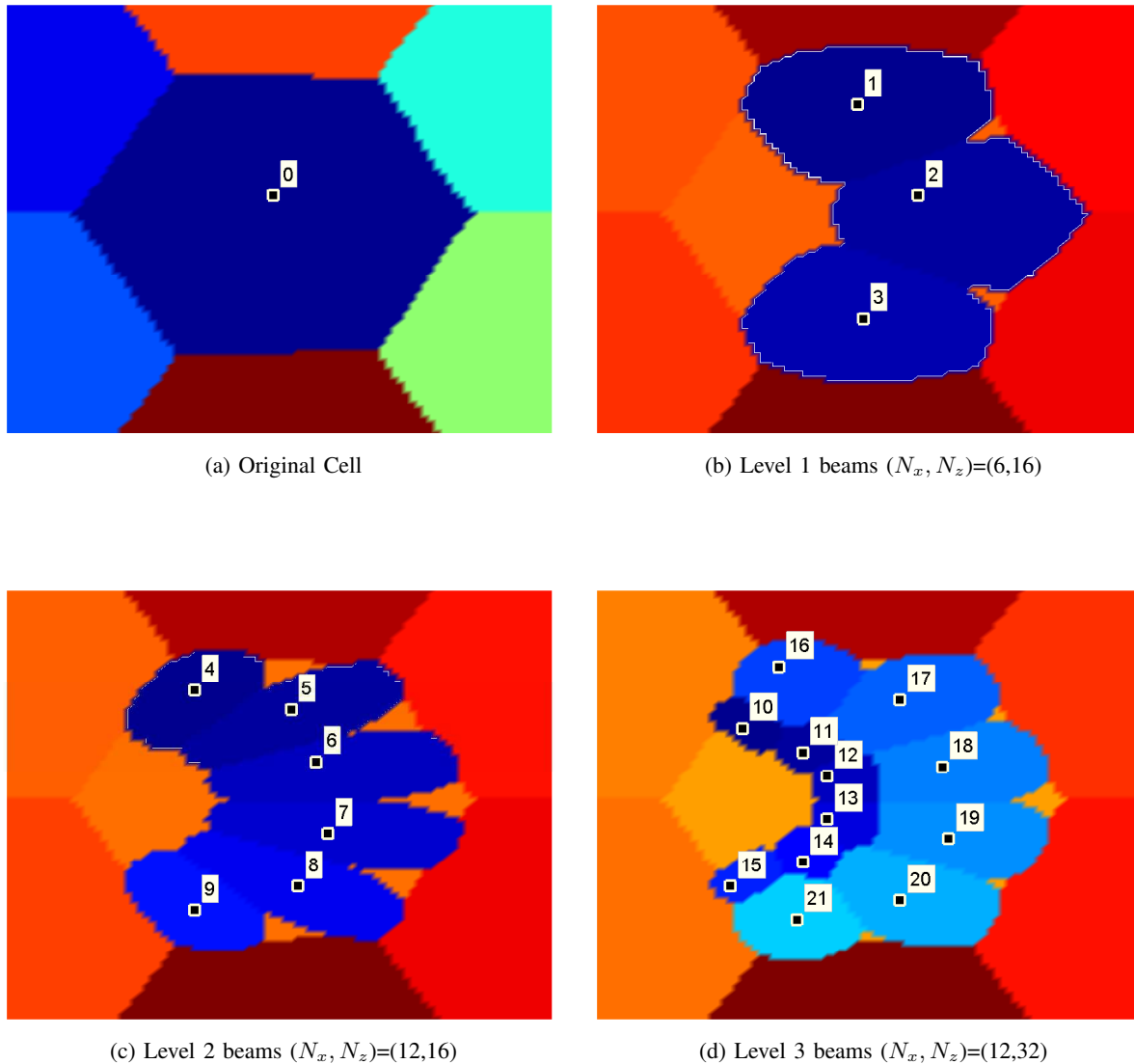


Fig. 4. Multilevel beam coverage maps for the mass event scenario

Figure 5 presents the beam selection algorithm performed according to (16) for a given user. The SINR of the selected user gradually increases from 7.75dB to 17.38dB at three iterations, i.e. by a factor of 9. It is noted that the SINR gains are expected to be even higher for cell edge users.

The antenna diagrams corresponding to the selected beams in each level in Figure 5 are presented in Figure 6. These diagrams were designed according to the optimization problem

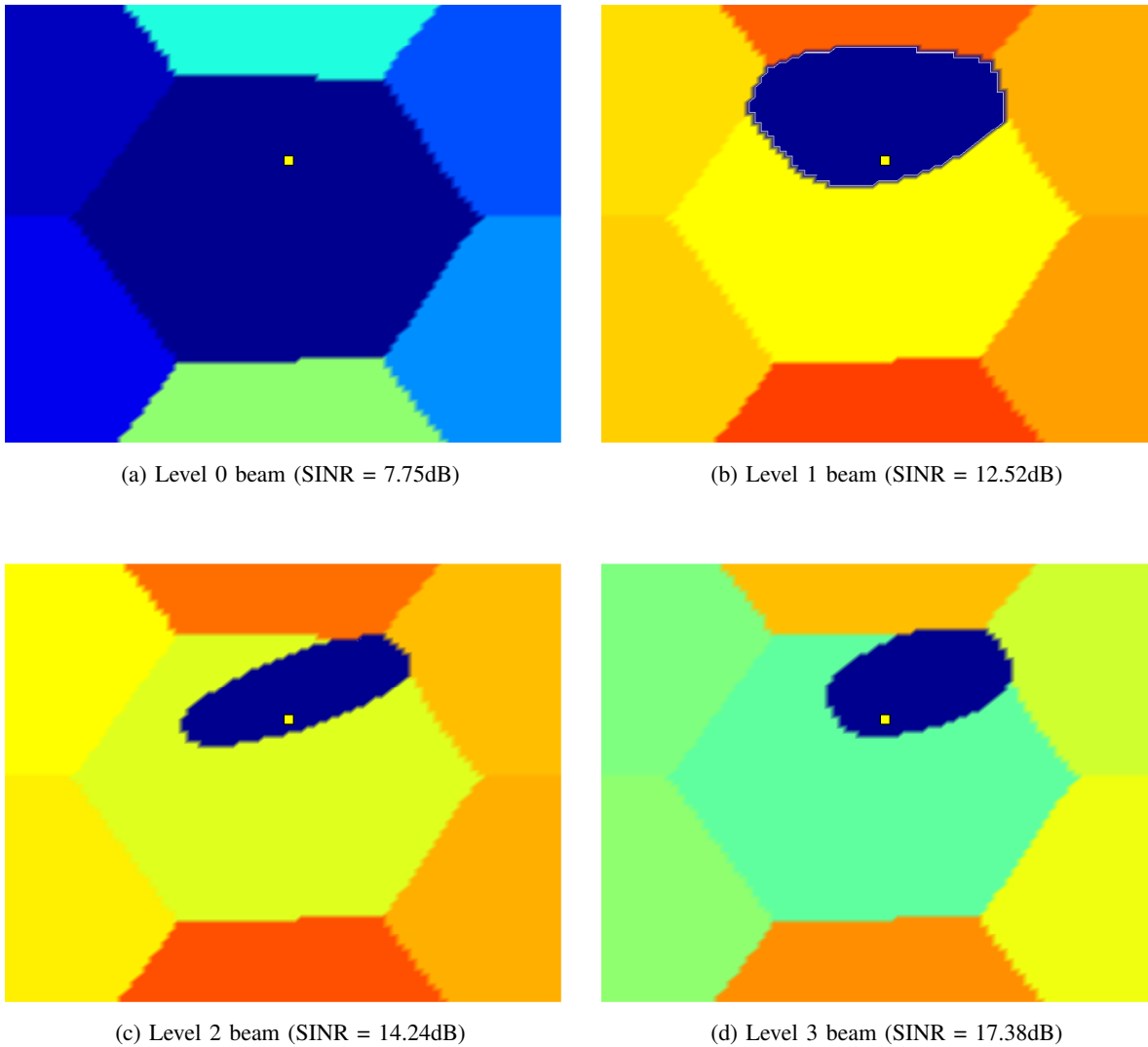


Fig. 5. Successive narrowing of the beam for a given user

(13), with the side-lobe level constraint (13c) of $Th = 30dB$. One can see that the beam width of the main lobe gets narrower in elevation or azimuth plane and the maximum gain increases (from 23.76dB to 30.2dB) with the beam level. The antenna diagram for level 0 which correspond to the full cell coverage is omitted.

2) *Performance results*: We next evaluate the performance of the multilevel beamforming for the mass event urban scenario. We use the Nakagami-m distribution which models fast-fading in environments with strong LoS component and many weaker reflection components. The *shape*

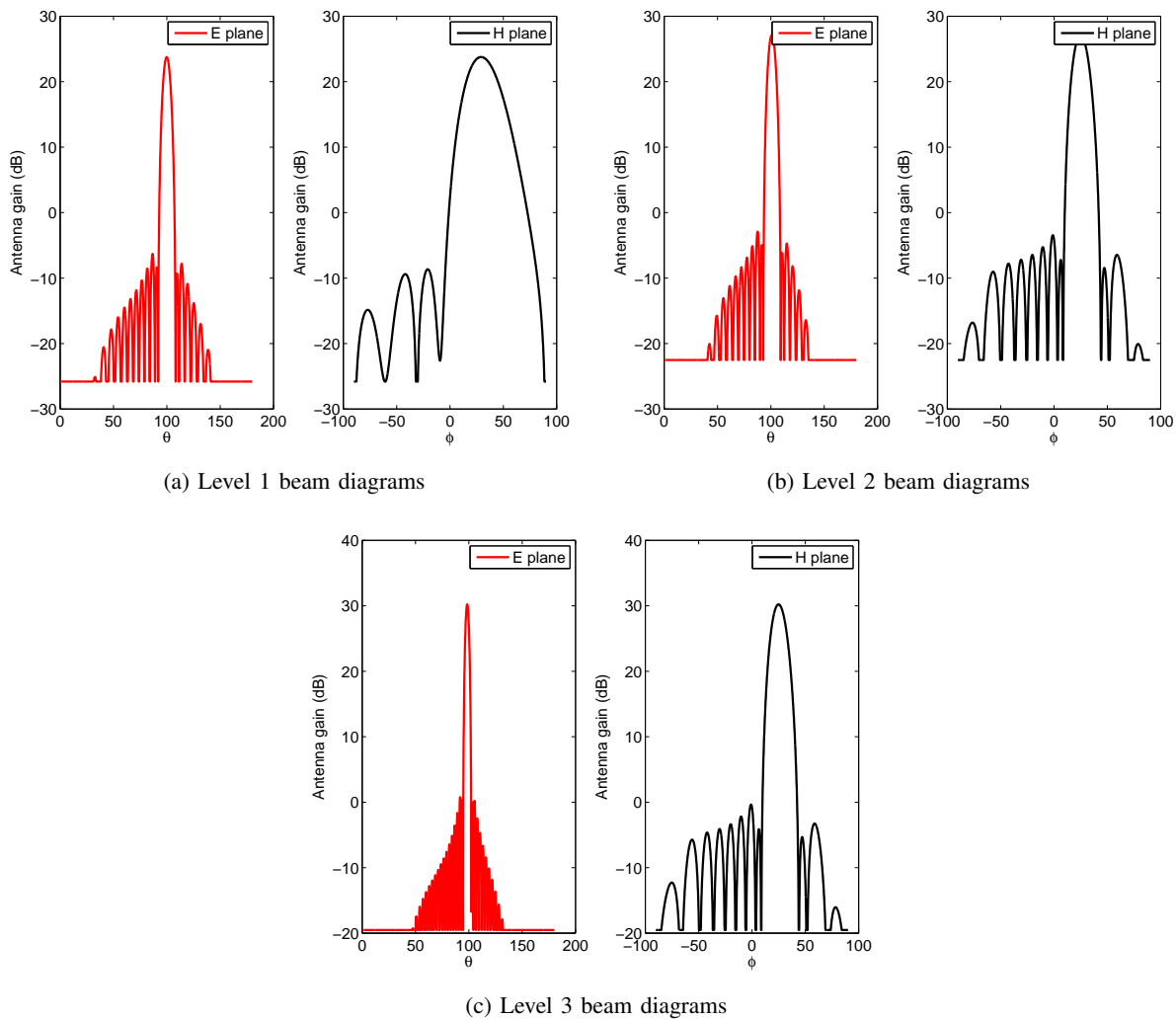


Fig. 6. Antenna diagrams for a given user's best beam in each level.

parameter m dictates the contribution of the LoS component in the overall signal. For $m = 1$, there is no LoS component and the fast fading reduces to a Rayleigh distribution. As m grows to infinity, the LoS component gradually becomes preponderant. We consider various Nakagami- m fading scenarios with $m = 2, 5$ and 10 , and the no-fading case (corresponding to $m = +\infty$). We do not consider the $m = 1$ case due to the open environment considered in the scenario. The simulation parameters for the scenario are summarized in Table II.

Figure 7 presents the frequencies of selected beams throughout the simulation. As expected, beam 17 which covers most of the hotspot region (see Figures 3 and 4d) is the most frequently selected. So the beam selection algorithm successfully locates the traffic in the direction of the

TABLE II. NETWORK AND TRAFFIC CHARACTERISTICS FOR THE MASS EVENT SCENARIO

Intersite distance	500 m
Nakagami-m shape parameter	2, 5 or 10
Traffic spatial distribution	Gaussian Hotspot + Uniform (see Figure 3)

hotspot and adjusts the beam width without any prior knowledge of the hotspot location and size.

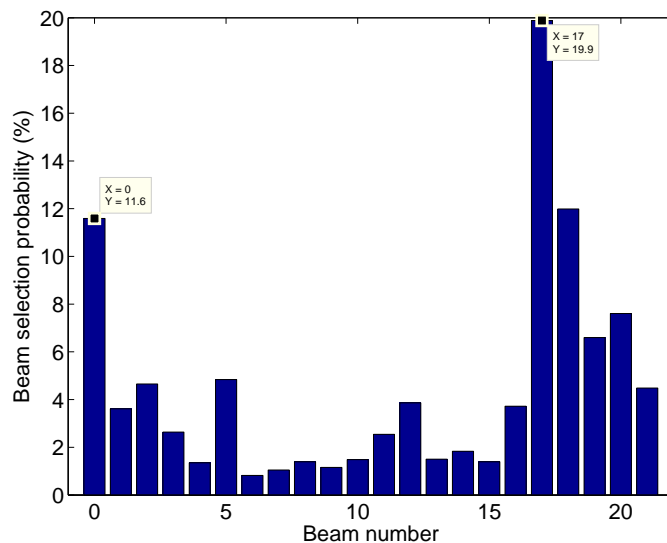


Fig. 7. Histogram of selected beams throughout the simulation: X is the beam number (see Figure 4) and Y - its selection probability.

Table III presents the Mean User Throughput (MUT), the Cell-Edge Throughput (CET) and the Power Consumption (PC) obtained for the various shape parameters of the Nakagami-m fading distribution, with and without (denoted respectively as 'w.' and 'wo.' in Table III) the multilevel beamforming. For example, in Table III, '2 wo.' means $m=2$ without multilevel beamforming. The PC is evaluated using the approximate linear PC model given in [11, Eq. (4-3)]

$$P_c = P_0 + \alpha P \quad (17)$$

TABLE III. PERFORMANCE GAIN USING MULTILEVEL BEAMFORMING FOR THE MASS EVENT SCENARIO

m	MUT (Mbps)	CET (Mbps)	PC (W)
2 wo.	7.64	1.78	397
2 w.	21.49 (181%)	5.52 (210%)	334 (-15.92%)
5 wo.	7.21	1.35	400
5 w.	22.33 (210%)	5.59 (312%)	331 (-17.24%)
10 wo.	6.97	1.18	402
10 w.	22.43 (222%)	5.31 (349%)	331 (-17.51%)
$+\infty$ wo.	4.99	0.51	417
$+\infty$ w.	21.85 (337%)	4.75 (822%)	334 (-19.98%)

where $P_0 = 260\text{W}$ is the PC for zero-load, $\alpha = 2 \times 4.7$ is the scaling factor term for an antenna with two-transmission chains and P is the total transmit power when serving a user with the entire bandwidth.

The performance results show particularly high gain brought about by multilevel beamforming. The MUT is improved by a factor varying from 2.81 to 4.38, the CET - from 3.1 to 9.22, and the PC is reduced by 15.9 to 20 percent for m varying from 2 to $+\infty$ respectively. The difference in performance gain between MUT and CET is due to the fact that cell edge users have initially low SINR and their SINR gain with beam focusing is larger. The PC is reduced due to the significant reduction in the sojourn time of the users so the BS transmits less often.

The performance gains increase with the value of m , namely with the importance of the LoS component relative to the multipaths' components. It is recalled that in an environment rich of scatterers, the initial level of beams (i.e. level 0 in Figure 2) will benefit from higher diversity gain by using an opportunistic scheduler (e.g. Proportional Fair (PF)) and therefore the gain obtained by the multilevel beamforming is smaller. This observation further supports the claim that the the multilayer beamforming is of particular interest for open type of environment having a significant LoS propagation.

TABLE IV. NETWORK AND TRAFFIC CHARACTERISTICS FOR THE RURAL SCENARIO

Intersite distance	1732 m
Fast-fading	None
Traffic spatial distribution	uniform
Arrival rate	2.5 users/s/km ²

B. Rural scenario

The simulation parameters for the rural scenario are summarized in Table IV. Unlike the mass event urban scenario, the bigger dimensions of the cell make vertical beam separation complex. A modification of the beam direction in elevation by a fraction of a degree results in significant difference in its coverage. For this reason, we consider multilevel beamforming in the horizontal (azimuth) plane, as shown in Figure 8.

For the sake of brevity, fast-fading is not considered here. However, similar results as those presented for the mass event urban scenario (see Section IV-A2) are expected, with performance gains increasing with the shape parameter m of the Nakagami- m fading.

Table V compares performance results for MUT, CET, and PC using different numbers of beamforming levels. The performance of level k corresponds to the case where equation (16) is applied to a highest beam level set to k . The performance gain are very high also in the rural scenario. For example, for three levels of beams, MUT and CET are increased by 238 and 501 percent. It is noted that the gain achieved is lower than that obtained in the mass event urban scenario. The reason for this is the smaller number of antenna elements used in the rural scenario which results in lower antenna gains. For example, in the third (highest) level, the number of antenna elements are $(N_{x,max}, N_{z,max})=(20,14)$ and $(N_{x,max}, N_{z,max})=(12,32)$ in the rural and the mass event scenarios, respectively.

V. CONCLUSION

A design framework for beam focusing using antenna arrays has been presented in this paper. In order to reduce the search complexity among all possible beams when a user is scheduled, a multilevel beamforming strategy has been adopted in which the best beam is

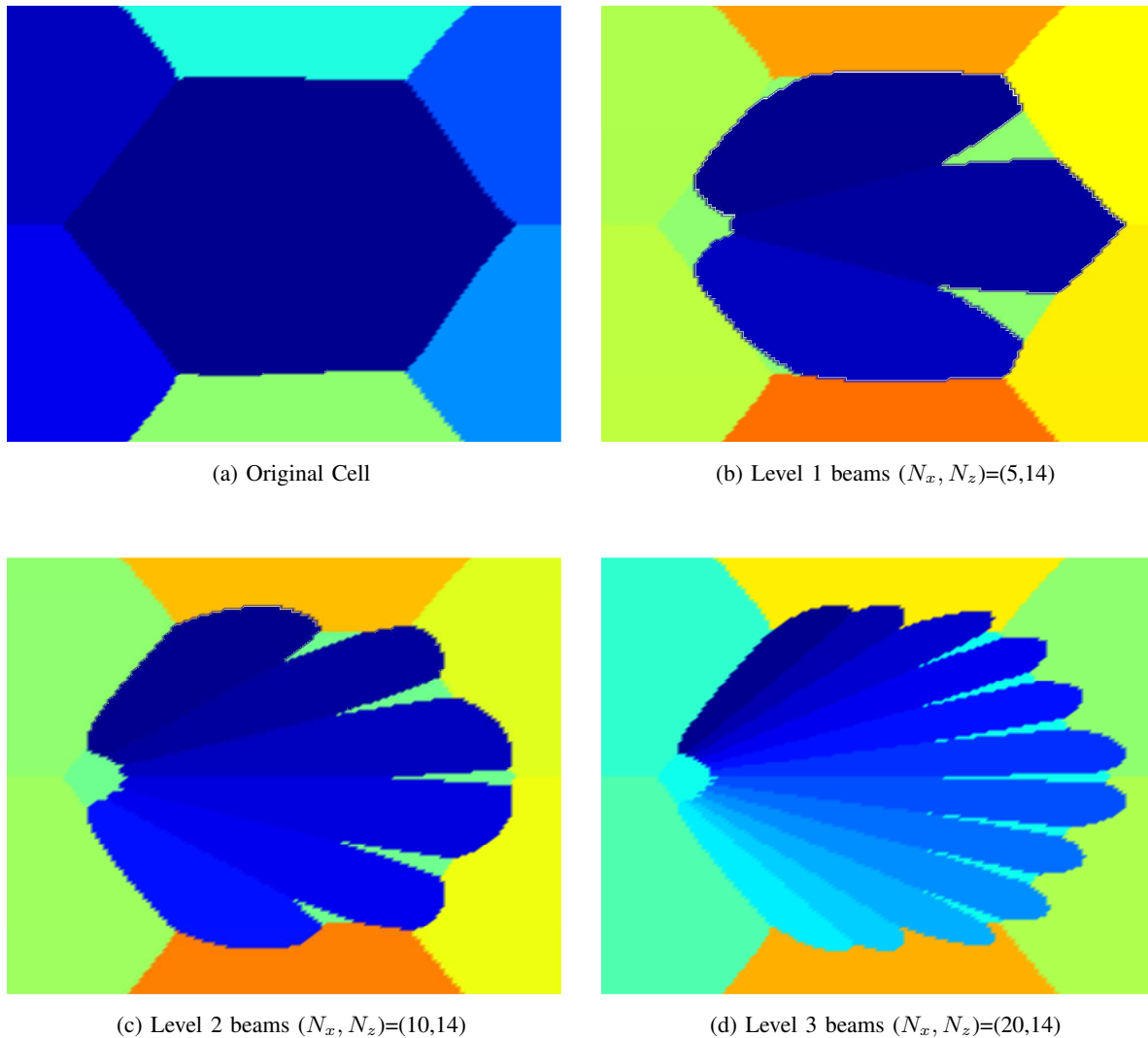


Fig. 8. Coverage maps for different beamforming levels for the rural scenario

iteratively selected for each level based on the user CQI. The multilevel beams' codebook can be constructed offline, as an optimization problem, taking into account coverage and interference constraints in each level. A higher level beam covers a fraction (e.g. half) of its lower level parent beam. The numerical results show very high performance gains brought about by the multilevel beamforming, both in terms of throughput and power consumption. Two scenarios have been evaluated: a mass event urban scenario and a rural scenario. The multilevel beamforming solution is well adapted to the FDD technology, and provides highest gains in environment with

TABLE V. PERFORMANCE GAIN USING MULTILEVEL BEAMFORMING FOR THE RURAL SCENARIO FOR DIFFERENT BEAM LEVELS

	MUT (Mbps)	CET (Mbps)	PC (W)
Level 0	4.66	0.43	421
Level 1	9.9 (112%)	1.15 (168%)	388 (-7.93%)
Level 2	13.23 (184%)	1.96 (360%)	369 (-12.3%)
Level 3	15.78 (238%)	2.57 (501%)	356 (-15.42%)

significant LoS component and low level of multipath propagation. To achieve highly focused beams, antenna arrays with a large number of radiating elements is required. Hence higher frequency envisaged in 5G spectrum evolution will make this technology particularly attractive.

REFERENCES

- [1] A. Osseiran, F. Boccardi, V. Braun, K. Kusume, P. Marsch, M. Maternia, O. Queseth, M. Schellmann, H. Schotten, H. Taoka *et al.*, “Scenarios for 5G mobile and wireless communications: the vision of the METIS project,” *Communications Magazine, IEEE*, vol. 52, no. 5, pp. 26–35, 2014.
- [2] Y. Chen, F. Han, Y.-H. Yang, H. Ma, Y. Han, C. Jiang, H.-Q. Lai, D. Claffey, Z. Safar, and K. Liu, “Time-Reversal Wireless Paradigm for Green Internet of Things: An Overview,” *Internet of Things Journal, IEEE*, vol. 1, pp. 81–98, Feb 2014.
- [3] C. Oestges, J. Hansen, S. M. Emami, A. D. Kim, G. Papanicolaou, and A. J. Paulraj, “Time reversal techniques for broadband wireless communication systems,” in *European Microwave Conference (Workshop), Amsterdam, The Netherlands*, 2004, pp. 49–66.
- [4] D.-T. Phan-Huy, S. Ben Halima, and M. Helard, “Dumb-to-perfect receiver throughput ratio maps of a time reversal wireless indoor system,” in *Telecommunications (ICT), 2013 20th International Conference on*. IEEE, 2013, pp. 1–5.
- [5] D.-T. Phan-Huy, M. Sternad, and T. Svensson, “Adaptive large MISO downlink with Predictor Antenna array for very fast moving vehicles,” in *Connected Vehicles and Expo (ICCVE), 2013 International Conference on*. IEEE, 2013, pp. 331–336.
- [6] X. Huang, Y. J. Guo, and J. D. Bunton, “A hybrid adaptive antenna array,” *Wireless Communications, IEEE Transactions on*, vol. 9, no. 5, pp. 1770–1779, 2010.
- [7] S. Hur, T. Kim, D. J. Love, J. V. Krogmeier, T. A. Thomas, and A. Ghosh, “Multilevel millimeter wave beamforming for wireless backhaul,” in *GLOBECOM Workshops (GC Wkshps), 2011 IEEE*. IEEE, 2011, pp. 253–257.
- [8] A. Galindo-Serrano, S. Martinez Lopez, and A. Gati, “Virtual small cells using large antenna arrays as an alternative to classical HetNets,” in *First International Workshop on Intelligent Design and Performance Evaluation of LTE-Advanced Networks*, Glasgow, Scotland, May 2015.

- [9] A. Tall, Z. Altman, and E. Altman, "Virtual sectorization: design and self-optimization," in *5th International Workshop on Self-Organizing Networks (IWSON 2015)*, Glasgow, Scotland, May 2015.
- [10] R. R. Müller, M. A. Sedaghat, and G. Fischer, "Load modulated massive MIMO," in *IEEE GlobalSIP*, Atlanta, Dec. 2015.
- [11] M. Imran, E. Katranaras, G. Auer, O. Blume, V. Giannini, I. Godor, Y. Jading, M. Olsson, D. Sabella, P. Skillermark, and others, "Energy efficiency analysis of the reference systems, areas of improvements and target breakdown," Tech. Rep. ICT-EARTH deliverable, Tech. Rep., 2011.